

Prism Signal Processing of Coriolis Meter Data for Gasoline Fuel Injection Monitoring

^{a,b}Manus Henry, ^aFeibiao Zhou, ^aMichael Tombs, ^aFelix Leach, ^aMartin Davy, ^aMaruthi Malladi

^aUniversity of Oxford, UK

^bSouth Ural State University, Russian Federation

Corresponding Author: Manus Henry
Department of Engineering Science
Parks Road, Oxford OX1 3PJ.
Tel +44 1865 273913
Fax +44 1865 273021
manus.henry@eng.ox.ac.uk

Abstract

Prism Signal Processing is a new recursive FIR technique offering rapid filter design and calculation. It has previously been applied to Coriolis mass flow metering to generate fast (48 kHz) flow measurement updates, facilitating for the first time the direct mass flow measurement of individual fuel pulses injected into a laboratory diesel fuel injection test bench. In this paper we describe an augmented sensor signal filtering scheme which enables rapid tracking of the desired mode of flow tube vibration while notching out undesired modes. The new scheme is applied to a gasoline injection test bench where the vibrational interference is greater than for the previously described diesel system due to increased hydraulic shock. The paper presents experimental findings which illustrate the further challenges to be overcome in order to achieve the goal of traceable direct mass flow measurement of individual fuel injection pulses. For example, when a fuel pulse is shorter than the resonant period of the flow tube, the observed phase difference appears to show dependence on the instantaneous phase of the flow tube vibration.

Keywords: Prism signal processing; recursive FIR filtering; Coriolis mass flow metering; internal combustion engine; gasoline engine; fuel injection monitoring; dynamic response.

1. Introduction

Despite the projected future dominance of electric vehicles in many areas of the market, liquid hydrocarbon fuels will continue to be an important part of the energy supply for road transport, in particular for high-mileage applications [1]. Accordingly, Internal Combustion Engine (ICE) research and development remains an important pursuit, with an emphasis on increasing fuel economy and reducing emissions. Modern ICE vehicles (whether gasoline or diesel powered) routinely use high-pressure fuel injection systems with complex and varied fuel injection strategies. For maximum benefit, these strategies should be applied to the engine on a cycle-by-cycle, cylinder-by-cylinder basis, which in turn requires real-time measurement of the fuel flow rate of each injection event. For light transportation, each fuel injection typically has a duration of approximately 1 ms, but for larger engines this period may be extended by an order of magnitude or more. Direct measurement of fuel injection delivery would facilitate the efficiencies associated with closed loop control, including detecting and correcting for the effects of injector-to-injector variability. Poor or degraded injector performance in one or more cylinders, due to manufacturing tolerances, ageing, or internal fouling, is likely to dominate the total emissions from any vehicle.

Current techniques for fuel injection monitoring are, however, indirect and off-engine, where typically injectors are ‘characterized’ in engine laboratory trials [2]. Measurement methods include: the Zeuch [3] and Bosch [4] techniques, both of which infer flow rate from dynamic pressure measurements; electric charge-based techniques [5, 6]; laser Doppler techniques [7]; and momentum flux [8]. Some techniques are further able to examine hole-to-hole variations in fuel delivery from a multi-hole injector [9 -11]: this represents a level of detail beyond the scope of the current work, as explained below.

The motivation of the current work is to develop an instrumentation technique that, on the one hand, provides a directly traceable measurement of the injected fuel mass, but, on the other hand, is essentially non-intrusive, so that it is compatible with conventional engine operation, and could potentially be used in commercial vehicles. This implies an instrument placed upstream of the injector, but most of the current techniques require transducers placed downstream, replacing or substantially modifying the

conventional combustion chamber. As a consequence, such systems are typically used to characterise fuel injectors in engine laboratories, but are not suited to real-time, closed loop engine control. The creation of an upstream instrument will retain certain inherent limitations: it can only observe the flow entering, but not leaving, the injector, and hence details such as hole-to-hole variations in flow rate cannot be observed directly.

Modern Coriolis flow meters [12] offer the potential for direct and traceable mass flow metering, but the fuel injection application has many challenges. These include high levels of vibration, electrical noise, pulsating flows and very high transient pressures (up to 300 MPa). In addition, measurement update rates must be increased from typically 10 Hz (as produced by current commercial Coriolis meters) to 50 kHz or more. A Coriolis mass flow meter consists of a mechanical flow tube, placed in line with the process pipework, together with the electronic transmitter which controls the flow tube and generates the measurement data. The transmitter therefore combines measurement and control functionality, as it is required to initiate and maintain the oscillation of a vibrating flow tube at a selected natural mode of vibration [13]. Two velocity sensors monitor the flow tube vibration, where the (common) resonant frequency is a function of the fluid density, while the phase (or more strictly the time) difference between the two sensor signals yields the mass flow rate. The rest of the paper will assume a reasonable familiarity with the operation and signal processing issues associated with Coriolis mass flow metering – reference [12] provides a thorough introduction to the technology and recent developments in the field, while [13] provides an overview of the key measurement and control tasks performed by the transmitter.

Our earlier work on the application of Coriolis metering to diesel fuel injection in laboratory trials is described in [14, 15], and aspects of the current work, such as the experimental setup, are similar and not repeated in detail here. We use our own prototype transmitter based on the Zynq system-on-chip device [14] which facilitates the development of PSP algorithms and generation of fast measurement updates. This transmitter has been coupled to a commercial Rheonik RHM 015 flow tube, rated to 100 MPa, which matches the operating range of the fuel injection operating environment. The flow tube is designed for high pressure applications such as dispensing hydrogen to vehicles, where batches of fluid are

transferred through the flow meter over the course of minutes, rather than milliseconds. The characteristics of this flow tube, in particular the resonant frequencies of its various modes of vibration, are therefore essentially designed to match its high pressure duty requirement, and the signal processing scheme in turn has been designed around the characteristics of the flow tube. While PSP implemented on a powerful transmitter can make significant progress towards tracking fuel injection pulses, in the longer term flow tube adaptations will also be required to provide a better solution, as discussed later in the paper.

Section 2 provides an overview of Prism Signal Processing. Section 3 gives an overview of how PSP can be used to match the signal processing requirements for the gasoline application, while Section 4 explains the dynamic notch filter design in detail. Section 5 presents a range of experimental results which demonstrate current limitations in measurement repeatability. Section 6 provides a summary, and discusses the further steps required to deliver traceable measurements in this application domain.

2. Prism Signal Processing

The Prism [16, 17] is a signal processing module (Fig. 1), consisting of two layers of cascaded integration blocks; it acts as an FIR filter with either one or two outputs, each of which has a linear phase response. Within each integration block the input signal is multiplied by a modulating sinusoid of frequency $m \times h$ Hz and integrated over a window of period $1/m$ s. The Prism's transfer functions are determined by m , the characteristic frequency, together with h , the harmonic number, a positive integer indicating how many periods of the modulating sinusoid occur over each integration period $1/m$. For a sinusoidal input signal with amplitude A , frequency f and initial phase ϕ_0 (i.e. the phase at $t = 0$)

$$s(t) = A \sin(2\pi ft + \phi_0) \quad (1)$$

the Prism outputs $G_s^h(t)$ and $G_c^h(t)$ are given by the following equations:

$$G_s^h(t) = A \text{sinc}^2(r) \frac{r^2}{r^2 - h^2} \sin(\phi(t) - 2\pi r) \quad (2)$$

and

$$G_c^h(t) = A \text{sinc}^2(r) \frac{hr}{r^2 - h^2} \cos(\phi(t) - 2\pi r) \quad (3)$$

where the instantaneous phase $\phi(t) = 2\pi ft + \phi_0$; $r = f/m$, is dimensionless frequency; and $\text{sinc}(x)$ is the normalized sinc function. The outputs G_s^h and G_c^h are orthogonal i.e. they form a sine/cosine pair; this orthogonality supports the calculation of properties such as the amplitude, frequency and phase of a sinusoidal input signal [16]. The frequency responses of the output functions G_s^h and G_c^h are shown in Fig. 2 for arbitrary frequency m , and $h = 1$ and 3. All functions have notches at multiples of m Hz, including at zero Hz, so that any DC component is removed by passing a signal through any Prism.

The Prism offers two advantages over the almost universally-applied convolution formulation of the FIR filter. Firstly, the Prism calculation is fully recursive so that the computational cost is low, and independent of the filter length. This ensures that computational resources are used efficiently, offering improved performance (for example more rapid measurement updates) for a given cost and/or power budget. Secondly, Prism filter design is simple: given the desired values of m and h , all that is needed is to calculate the linearly spaced sine and cosine values of the modulation functions. This contrasts with the often elaborate calculation of convolution FIR filter coefficients, particularly for high order [16]. Thus, using Prism Signal Processing (PSP) it is possible to create new filtering schemes in real time in response to changing signal processing requirements, for example in response to the detection of a fault condition. Networks of Prisms can be used to implement a variety of signal processing functions, including static and dynamic notch filtering (described below), band-pass filtering, and tracking, whereby the frequency, phase and/or amplitude of a sinusoidal signal can be calculated on a sample by sample basis [16]. Recent applications of PSP outside of the flow measurement field include pressure sensor validation [18], and condition monitoring of rotating machinery [19, 20]. The two-fold advantages of Prism filter design and evaluation are shown to be of particular advantage in [21, 22] where ultra-narrow band filters, with

lengths of up to several hundred million samples, have been designed and applied to live data in real time on a single FPGA; the equivalent conventional convolution form of FIR filter would require supercomputer resources to deliver the same data throughput.

The combination of design flexibility and low computational cost provides the motivation to investigate new measurement applications that might previously been considered infeasible. In this paper we describe how PSP techniques have enabled the analysis of Coriolis meter sensor signals to detect fuel injection pulses as short as 1 millisecond (ms) in a gasoline fuel injection experiment, despite the presence of high levels of mechanical vibration. This is seen as a useful step towards the goal of providing traceable, direct mass flow measurement of fuel injection in internal combustion engines, firstly in laboratory instruments and ultimately in production vehicles.

3. Notch Filtering for Fuel Injection monitoring

Fig. 3 shows the unfiltered (green) and filtered (blue) spectra of a Coriolis meter sensor signal from the selected flow tube when it is full of fuel but there is no flow, and where all mechanical operation is inactive other than the Coriolis meter itself (i.e. the fuel injection system is at rest). Note that the spectra from the two sensor signals show only minor differences, so the same filtering scheme is used for each, and only one sensor signal is shown throughout the paper.

In the unfiltered spectrum, the highest peak at around 149 Hz is the so-called drive mode, which is the natural mode of flow tube vibration actively maintained at a high and steady amplitude by the Coriolis drive control system [13]. Most of the other peaks present are harmonics of the drive mode (at around 300 Hz, 450 Hz, 600 Hz and 750 Hz). While the influence of harmonics must be managed in any Coriolis signal processing scheme, this is relatively straightforward to achieve, as typically the amplitude as well as the frequency is a fixed ratio of the drive mode itself. However, at around 245 Hz and 263 Hz there are spectral peaks corresponding to alternative modes of vibration of the flow tube, which act independently of the drive mode and are readily excited by mechanical noise, whether from the external environment, or

from fluid pulses within the flowmeter itself. The suppression of these other natural modes of vibration, whether by signal processing or mechanical means, is a common theme of Coriolis metering research and product development [23]. In the filtered spectrum, all components other than the drive mode have been largely suppressed, as desired.

Fig. 4 shows the corresponding unfiltered and filtered spectra when a stream of fuel injection pulses is passing through the flow tube. Here each pulse duration is 1 ms while the interval between each fuel pulse is 0.6715 s. Compared with the unfiltered spectrum in Fig 3, significant additional noise has been introduced by the fuel injection process. While the drive mode at 149 Hz is maintained at the same amplitude by the transmitter, the noise floor has risen two orders of magnitude from approximately 10^{-8} V to 10^{-6} V. The two modes of vibration around 250 Hz have risen by approximately an order of magnitude, while several peak frequencies, attributable to fuel injector operation, occur between 550 Hz and 700 Hz, with the peak at 674 Hz achieving an amplitude of 2 mV, compared to the drive mode amplitude of only 50 mV.

As discussed in [23], vibrational energy occurring as a peak in the Coriolis meter sensor signal spectrum can produce noise on the phase difference output; the physical positioning of the sensors on the flow tube is often used as a mechanical means of reducing the negative influence of the most common contaminating frequencies, which are usually the natural modes of vibration of the flow tube adjacent to the drive mode. Here, PSP notch filtering is used to suppress eight peaks, marked with circles in Fig. 4 in both the unfiltered and filtered spectra. These have been selected as targets for the PSP notch filtering technique to the high level of contamination each exerts on the phase difference calculation. One of these peaks is below the drive frequency at approximately 114 Hz. This corresponds to the difference (the ‘beat frequency’) between the drive mode (149 Hz) and a higher vibration mode (263 Hz). Its position close to the drive frequency results in relatively high levels of noise in the phase measurement calculation despite its relatively low amplitude; its location also makes it difficult to suppress while leaving the drive signal unaffected. Nevertheless, the spectrum of the filtered sensor data shows that all targeted frequency components have had their amplitudes reduced to no greater than around 3 μ V, including the beat

frequency at 150 Hz, the flow tube vibration modes around 250 Hz, and the engine vibration noise between 550 Hz and 700 Hz.

While the experimental setup providing this data is very similar to that used for the diesel injector (Fig. 6 in [14]), an important difference is the absence of a spill line in the gasoline rig. Diesel systems generally operate at higher pressures (100 – 300 MPa) than their gasoline equivalents, and diesel injectors usually include a ‘spill’ outlet which provides pressure relief during transients arising from the injector needle movement. Due to the lower pressures experienced in gasoline fuel injection (say 10-30 MPa). there is no need for such an injector spill. It is possible that in our previous diesel experimental flow loop the spill mechanism also provided a form of vibrational damping, as the level of mechanical noise observed in the gasoline experiments, absent the spill-line, is significantly higher than for the earlier diesel experiments: compare Fig. 4 with Fig. 5 in [14]. Accordingly, while in [14] a relatively simple Prism-based pre-filtering scheme is sufficient to suppress unwanted signal components while retaining the fuel pulses, a more elaborate scheme is required here.

As Fig. 4 illustrates, the signal processing challenge is significant, because on the one hand the level of mechanical noise is high, while on the other hand a key measurement requirement is to provide a dynamic response fast enough to detect millisecond fuel pulses. For example, the PSP bandpass filtering approach described in [21, 22] could readily remove all frequency components outside a narrow band around the drive frequency, but the resulting dynamic response would be too slow to detect the injections.

Fig. 5 shows a Prism-based filter designed to notch out undesired frequency components while retaining a fast dynamic response. This filter is more complex than that described in [14], reflecting the larger number of frequencies that must be suppressed to obtain good measurement in the gasoline test rig. The highest gain is given to the region of the drive frequency, around 150 Hz. The eight frequencies identified for notching in Fig. 4 are circled again in Fig. 5, and all have been successfully attenuated in this design. Note that Fig. 5 shows the relative gain against frequency. For any specific output frequency, (for example the resonant frequency of the flow tube) the absolute gain and phase delay of the sequence of filters may be calculated using simple formulae [16] so that compensation can be applied to obtain the

true values in the original sensor signal. This is an essential requirement for the Coriolis system, which is required to perform flow tube oscillation control based on real-time phase and amplitude data [13].

Finally, in this section, Figs. 6 and 7 show the phase difference calculated sample-by-sample for the unfiltered and filtered sensor data of Fig. 4. The phase difference (along with the frequency, amplitude and phase of each sensor signal) has been calculated sample-by-sample using the Prism-based Recursive Signal Tracker (described in [14]). The fuel pulse injection sequence begins at approximately $t = 3$ s. In Fig. 7, regular narrow pulses are discerned, while in Fig. 6, the unfiltered data results in a very noisy phase difference time series where the noise magnitude of around ± 2 degrees, is significantly larger than the peak fuel pulse height of around 0.4 degrees.

These results demonstrate the utility of the filtering scheme, which is described in Section 4.

Experimental results obtained using the fuel pulse measurements are presented in Section 5.

4. Dynamic Notch Filtering Design

The filter of Fig. 5 uses a Prism-based technique called Dynamic Notch Filtering (DNF), which is outlined in [16]. Here the mechanism is described in more detail, together with design issues to be considered when developing a filtering scheme for a difficult application like the gasoline fuel injection example.

The first step is to understand the mechanism and limitations of what may be termed static Prism-based filtering. If a Prism with parameters m and h , generating a single output (either G_c or G_s), is included in a signal path, the Prism acts as a filter, applying to the supplied input signal a linear phase delay and a frequency response of the type illustrated in Fig. 2, with notches at all multiples of m Hz. Although such static notch filtering is straightforward, it has certain limitations. The Prism frequency m must correspond to a whole number of samples, so that in practice notches can only be created at discrete frequencies.

Particularly where the sample rate is low relative to the desired notch frequency, the nearest implementable notch frequency may not deliver sufficient attenuation at the target frequency. Secondly,

creating notches at all multiples of m may be inconvenient, especially for low m , as this may interfere with higher frequency components that are to be tracked. Finally, each Prism adds a delay of $2/m$ seconds to the signal path with a corresponding delay to the dynamic response.

DNF is a means of using a static Prism filtering stage to create one or more additional notches without any further loss of dynamic response. This is achieved by using one or more additional Prisms in parallel with the first, with the same value of m but different values of h , and then combining all the Prism outputs with a suitably selected linear weighting. Here we will describe the simplest instantiation, where two Prisms are used to create one additional notch. For the fuel injection application where eight notched frequencies are required, this reduces the required number of filtering stages from eight to four.

The key idea of DNF is as follows. As shown in equations (2) and (3) and illustrated in Fig. 2, Prism outputs with the same value of m but different values of h have common notches at all multiples of m but different gains at all other frequencies. The outputs also have, for any selected frequency, the same phase offset (see equations (2) and (3)). Accordingly, as illustrated in Fig. 8, a suitably weighted sum of the G_c outputs of Prisms with common m and $h = 1$ and 2 respectively can cancel out the signal component (i.e. create an additional notch) at any desired frequency, f_{notch} .

The outputs of the two Prisms are, from equation (3), given by:

$$G_c^1(t) = A \text{sinc}^2(r) \frac{r}{r^2 - 1} \cos(\phi(t) - 2\pi r) \quad (4)$$

$$G_c^2(t) = A \text{sinc}^2(r) \frac{2r}{r^2 - 4} \cos(\phi(t) - 2\pi r) \quad (5)$$

$P(r)$, the ratio of the Prism output gains, can be calculated as a function of dimensionless frequency as follows:

$$P(r) = \frac{G_c^1(t)}{G_c^2(t)} = \frac{r^2 - 4}{2(r^2 - 1)} \quad (6)$$

Consider an input signal $s(t)$ consisting of a collection of desired frequency components $s_{pass}(t)$ together with an undesired frequency component $s_{notch}(t)$ at f_{notch} :

$$s(t) = s_{pass}(t) + s_{notch}(t) \quad (7)$$

The weighted sum of the two Prism outputs which removes frequency component $s_{notch}(t)$ with corresponding dimensionless frequency $r_{notch} = f_{notch} / m$ is given by:

$$s'(t) = G_c^{-1}(t) - P(r_{notch}) \cdot G_c^2(t) \quad (8)$$

In the resulting output signal $s'(t)$ there are notches at f_{notch} and at all multiples of m , so that $s_{notch}(t)$ is removed. The technique is called *Dynamic* Notch Filtering because the two Prism outputs can be used to notch any frequency, depending only upon the weighting applied, and so f_{notch} can be selected and varied in real time. Indeed, from the same two Prism outputs, separate time series can be generated with different weightings and hence different notch frequencies, for example in order to split a signal into two separate frequency components, as described in [16].

In the fuel injection application, eight frequencies are notched, arranged as four DNF stages (Fig. 9). The raw sensor signal is passed through each stage before being sent to a tracker, which calculates the frequency, phase and amplitude of its input, on the assumption that the post-filtered signal is a simple sinusoid with only one frequency component. The concatenation of all four DNF stages in Fig. 9 results in the overall frequency response shown in Fig. 5. Table 1 lists these frequencies as they are paired for the application of DNF. The frequency responses of the first and last stages are shown in Figs. 10 and 11.

Table 1: Notched frequencies

Static notch frequency m (Hz)	DNF frequency (Hz)
245.0	683.7
262.6	580.8
447.1	298.0
622.9	114.3

In Fig 10, the static notch frequency m is 245.0 Hz, and the DNF frequency is 683.7 Hz – both frequencies are marked with red circles. The frequency response of the output consists of regular notches at all multiples of m as well as the DNF frequency. As the DNF frequency is higher than m , this results in more rapid attenuation of high frequencies. By contrast, in Fig. 11, the DNF frequency (114.3 Hz) is lower than the m (622.9 Hz). Again all multiples of m are notched, along with the DNF frequency, but the weighted combination results in a much slower attenuation of high frequency components.

The DNF technique addresses, to some degree, each of the previously mentioned limitations of static Prism-based notch filtering. Firstly, while the selected value of m must correspond to a discrete number of samples, there is no restriction on the dynamic notch frequency value, which can be targeted exactly using the appropriately weighted combination of the two Prism outputs. Secondly, while all multiples of the selected m value are notched, there are no additional notches at multiples of the dynamic notch frequency, so this technique is particularly suited to targeting low frequencies. Finally, although the technique requires the computational load associated with the two Prisms of Fig. 8, the time delay and dynamic response is equivalent to only a single Prism with its m value.

Given eight desired notch frequencies, there are many possible ways of pairing them in four DNF stages - Table 1 lists a combination which has been selected to provide a balance between achieving high gain in the region of the drive frequency (with low gain elsewhere), and a fast response. As illustrated in Figures 10 and 11, pairing a lower static frequency with a higher DNF frequency results in a poorer dynamic response but rapid attenuation of high frequencies (Fig. 10), while pairing a high static frequency with a low DNF frequency gives a fast dynamic response but also relatively low gain at the drive frequency compared with higher frequencies (Fig. 11). This particular combination of high and low static notch frequencies has been found (by trial and error) to deliver acceptable filtering performance. The delay for the filter is 23.5 ms, while the total delay for each of the individual Prisms is 54 ms.

The signal processing design approach adopted here implicitly assumes essentially fixed frequencies and hence relatively small variation in fluid density, which is the primary cause of resonant frequency

variation for a given flow tube design. In practice this assumption is warranted for a well-specified fuel, but where density variation is expected (for example where a system may be used on different fuel specifications), then alternative filter designs with the same structure but different characteristic frequencies can be assembled. Variations in temperature, with its impact on flow tube stiffness as well as fluid density, is more likely in an engine test environment, and this could lead to some corresponding modest variation in resonant frequency.

The Prism-based filtering and tracking scheme has been implemented using a commercial high pressure flow tube connected to a prototype transmitter based on a dual-ARM core Zynq FPGA. Real-time processing, including flow tube control, is carried out by one ARM core, while the second core provides system functions including data archiving and a Web interface.

The development and testing of the PSP scheme, operating in real-time in the prototype transmitter, has followed well-established practice, as follows:

- 1) Simulation studies have been carried out to evaluate performance over a variety of noise conditions and dynamic flow changes;
- 2) The real-time performance has been evaluated using signal generator input (a useful development stage which allows the evaluation of measurement performance independently from the requirement for flow tube control [13]); and
- 3) Conventional calibration tests have been carried out at static flow rates against a traceable master meter, demonstrating mass flow performance with uncertainty ($k = 2$) of approximately 0.1 % over at least a 10:1 turndown, covering the peak flow rates used in the fuel injection experiments.

5. Experimental Results

As Fig. 7 shows, the DNF filtering technique results in the successful detection of fuel injection pulses. However, there are clear limitations to the current technique, as discussed in this section.

The first limitation is that each fuel pulse is spread out in time by the dynamic response of the Prism filtering, and possibly also by the flow tube dynamics. Fig. 12 shows a close-up of the phase difference measurement obtained over the course of an individual fuel pulse (from Fig. 7). The true pulse duration is 1 ms, but as measured by the period of continuously positive phase difference starting at $t = 4.918\text{s}$, the pulse length has been extended to approximately 10.5 ms.

The more serious limitation is the non-repeatability of the phase difference measurement, which is believed to be due to the flow tube dynamics when responding to fuel pulses which are significantly shorter than the period of the flow tube vibration mode. The clearest indication of non-repeatability is that fuel pulse trains induce large zero offsets in the phase difference measurement, where the zero offset appears to show strong dependency on the instantaneous phase of the flow tube vibration. Figs. 13 – 15 demonstrate one aspect of the problem, while Figs. 16 and 17 present the issue in its most general form. In all the examples presented so far, including Figs. 13 – 15, the time period between fuel pulse injections has been carefully selected to be as close as possible to an exact multiple of the flow tube period. This represents a significant restriction with respect to engine operation, of course, as in practice the fuel injection period may vary within a continuous range of rpm values. Despite this restriction, basic repeatability is not achieved, as demonstrated in the differences between Fig. 13, 14, and 15. The data comes from a set of experiments where the pulse duration is 1.5 ms and the period between pulses is 40.3 ms, i.e. corresponding to exactly 6 flow tube periods. Each graph shows the phase difference and the amplitudes of the two sensor signals over a 0.5 s window of data for each experiment starting at $t = 11\text{s}$. Note that before and after the fuel pulse train the parameters have steady values as follows: the phase difference is 0.0 degrees, Sensor Voltage 1 is 0.0601 V, and Sensor Voltage 2 is 0.0599 V.

In Fig. 13, the phase difference retains a baseline (i.e. has the highest data density, where this is taken as an indication of zero offset) around 0° , with peak values at around 0.6° and a minimum value of around -0.1° . The Sensor Voltage 1 Amplitude drops when the pulse train starts, settling to a baseline value of around 0.0598 V with peak values of 0.0601 V. By contrast the Sensor Voltage 2 amplitude rises at the beginning of the sequence, with the baseline at 0.0602V and equidistant peaks and troughs at

approximately 0.0604 V and 0.0600 V respectively. Each of the three measurements shows a repeatable pattern of behavior for each fuel injection event. The phase relationship between the measurements is revealing. At $t = 11.1$ s, for example, it can be seen that the SV1 amplitude is at its maximum, and the SV2 amplitude is at its minimum, just as the phase difference is about to start climbing its next peak. By contrast, at $t = 11.35$ s, SV1 is at its minimum, SV2 is at its maximum, and the phase difference pulse has just ended. Accordingly, the phase pulse takes place during a period of rapidly dropping SV1 and rising SV2.

Fig. 14 shows data from another experiment, carried out a few minutes later, with identical nominal conditions, fuel pulse duration and period between pulses. Here a different pattern of behavior is established. Most notably, the phase difference itself settles to a baseline of around -0.3° and its peak values only just exceeds 0° . There are some similarities with the behavior in Fig 13 – for example, the phase difference peaks remain correlated with rapid fall in SV1 and a rapid rise in SV2, for example at $t = 11.2$ s. However, there appears to be strongly negative correlation between the two sensor amplitudes patterns of SV1 and SV2, whereas in Fig 13 the two waveforms have quite different shapes.

In Figure 15, a further similar experiment is shown where, after the onset of the fuel pulses, the SV1 amplitude remains approximately constant, the SV2 amplitude goes high and drifts downwards, while the phase difference exhibits a large positive bias of around $+0.4^\circ$, reaching peak values in excess of 1° . Once again the peaks in phase difference (for example at $t = 11.4$ s) are associated with a rapid drop in SV1 and a rapid rise in SV2, while the waveforms of the two sensor signals are distinct both from one another and from the earlier experiments.

From a measurement perspective, the problem is clear: for nominally identical conditions, distinct phase difference results are obtained. Not only are separate baseline (i.e. zero offset) values established in each case, but the difference between the baseline and peak value is 0.6° in Figs. 13 and 15, but only 0.3° in Fig. 14. Divergent behaviour is also shown by the two sensor amplitudes, which suggests that the flow tube dynamics is playing an important role. One possible causative factor is the phase of the flow tube vibration when the injection pulse starts. Note that in the current experimental setup this initial phase is

random, as there is no timing synchronization between flow tube phase and pulse sequence initialization. However, setting the interval between pulses to be a whole number of flow tube periods ensures that the initial phase is the same for each fuel pulse in the sequence. This initial phase could be influential in how the sensor amplitudes respond, which in turn might affect the phase difference characteristics. For example, in the three examples shown, the peak phase differences occur at different points in the flow tube cycle, where the SV1 phase is approximately 120° , 33° and 45° respectively.

If the constraint is removed that the time interval between pulses should be a whole number of flow tube vibration periods, then more complex behavior is observed, as shown in Figs. 16 and 17. Here, the time between pulses has been extended from 40.15 ms to 40.3 ms, i.e. slightly longer than 6 periods of flow tube oscillation. In response, the flow tube generates a complex pattern of phase difference and sensor voltage amplitudes, which are shown in more detail in Fig. 17. The basic variation is sinusoidal in each case, with the pulse shape of each parameter gradually changing over the course of the cycle. The evolving pulse shapes include similar patterns to those shown statically in Figures 13, 14 and 15, although strong matching has not been found. The two second period of data shown corresponds approximately to one cycle of the parameter variation, and it can be seen that both the mean value and pulse shape of each parameter are roughly the same at $t = 11$ and $t = 13$ s. In experiments with different time periods between pulses, the period of this characteristic cycling also varies, returning to near static behavior when the pulse interval matches a whole number of flow tube periods.

The experimental work has demonstrated that while the PSP technique has enabled the detection of individual fuel pulses, further developments are necessary to generate a repeatable flow estimate with low uncertainty. In [24], we describe a first analysis to improve the repeatability of the phase difference calculation in these experiments, by assuming the phase difference is a function of the instantaneous phase.

6. Summary and Discussion

This paper has described how Prism signal processing may be used to create a notch filtering scheme facilitating the active tracking of short fuel pulses in real time. Prism signal processing renders the design of individual Prisms straightforward, and the recursive calculation means that the computational burden is low. Experimental results demonstrate, however, that where the fuel pulse duration is significantly shorter than the period of flow tube vibration, basic repeatability is not achieved, whereby the observed phase difference appears to be a function of the instantaneous flow tube phase.

Consideration of the various possible causes of the observed non-repeatable behaviour leads to proposals for next steps for improving the flow measurement performance for this difficult application, including the following:

1) CFD modelling of short fuel pulses on the flow tube dynamics could provide insight into the physical relationship between amplitude, phase and phase difference behavior in these conditions. Such studies could inform correction calculations and perhaps suggest improved flow tube control strategies.

2) The current paper has described Prism signal processing techniques for tracking fast flow transients. Other signal processing techniques may be developed or adapted for such applications – for example [25] described a complex bandpass technique intended for tracking rapid transients in two-phase flow conditions, and compares its performance with well-established Coriolis tracking techniques via simulation. It is an open question whether alternative techniques would exhibit phase dependency for short flow transients.

3) In the authors' view the surest means to improve measurement quality for fast flow transient applications is to develop flow tubes with substantially higher resonant frequencies so that typical fuel pulses are of the same duration or longer than the flow tube period of oscillation. While micro-machined Coriolis meters have been reported in the literature with resonant frequencies of 3 kHz or higher [26, 27], which may be suited to other applications with fast transient flow, the fuel injection application has additional challenges such as high external vibration and a high pressure requirement.

A particular advantage of PSP is its recursive FIR structure, which provides both numerical stability and low computational cost, so that, as described in [21, 22], a PSP filter and tracking scheme of similar complexity to the one described can operate in real time at 20 MHz on an FPGA. In our view, PSP provides an appropriate data processing solution for transient fuel injection tracking, assuming the availability of suitably specified and high resonant frequency flow tubes. We are currently working with partners to develop a high pressure flow tube with a target resonant frequency of 1 kHz, alongside a transmitter architecture providing > 500 kHz, 24-bit sampling, to provide an improved fuel injection tracking prototype.

Acknowledgement

The work described in this paper was supported by funding from the Advanced Propulsion Centre Ltd, UK (grant number: PGC015) BP, EPSRC (grant number: EP/R512333/1-1939160), Keble College UK (grant number: KSRG066), and Rheonik, Germany.

References

- [1] G. Kalghatgi, “Is it really the end of internal combustion engines and gasoline in transport?”, *Appl. Energy*, vol. 225, no. April, pp. 965–974, 2018.
- [2] B. Mohan, J. Du, J. Sim, and W. L. Roberts, “Hydraulic characterization of high-pressure gasoline multi-hole injector,” *Flow Meas. Instrum.*, vol. 64, no. October, pp. 133–141, 2018.
- [3] W. Zeuch, Neue verfahren zur messung des einspritzgesetzes und der einspritz- regelmäßigkeit von diesel-einspritzpumpen, *Mot. Z.* 22 (9) (1961) 344–349.
- [4] W. Bosch, The fuel rate indicator: a new measuring instrument for display of the characteristics of individual injection. Tech. Rep.; SAE Technical Paper; 1966.
- [5] M. Marčič, “A new method for measuring fuel-injection rate,” *Flow Meas. Instrum.*, vol. 10, no. 3, pp. 159–165, 1999.
- [6] M. Marčič, “New diesel injection nozzle flow measuring device,” *Rev. Sci. Instrum.*, vol. 71, no. 4, pp. 1876–1882, 2000.
- [7] C. Crua and M. R. Heikal, “Time-resolved fuel injector flow characterisation based on 3D laser Doppler vibrometry,” *Meas. Sci. Technol.*, vol. 25, no. 12, 2014.
- [8] R. Payri, J. M. García, F. J. Salvador, and J. Gimeno, “Using spray momentum flux measurements to understand the influence of diesel nozzle geometry on spray characteristics,” *Fuel*, vol. 84, no. 5, pp. 551–561, 2005.
- [9] M. Marčič, “Measuring method for diesel multihole injection nozzles,” *Sensors Actuators, A Phys.*, vol. 107, no. 2, pp. 152–158, 2003.
- [10] T. Luo, S. Jiang, A. Moro, C. Wang, L. Zhou, and F. Luo, “Measurement and validation of hole-to-hole fuel injection rate from a diesel injector,” *Flow Meas. Instrum.*, vol. 61, no. March, pp. 66–78, 2018.

- [11] L. Y. Zhou, S. F. Dong, H. F. Cui, X. W. Wu, F. Y. Xue, and F. Q. Luo, "Measurements and analyses on the transient discharge coefficient of each nozzle hole of multi-hole diesel injector," *Sensors Actuators, A Phys.*, vol. 244, pp. 198–205, 2016.
- [12] T. Wang and R. Baker, "Coriolis flowmeters: A review of developments over the past 20 years, and an assessment of the state of the art and likely future directions," *Flow Meas. Instrum.*, vol. 40, pp. 99–123, 2014.
- [13] M. Zamora and M. P. Henry, "An FPGA implementation of a digital Coriolis mass flow metering drive system," *IEEE Trans. Ind. Electron.*, vol. 55, no. 7, 2008.
- [14] F. Leach, S. Karout, F. Zhou, M. Tombs, M. Davy, and M. Henry, "Fast Coriolis mass flow metering for monitoring diesel fuel injection," *Flow Meas. Instrum.*, vol. 58, pp. 1–5, 2017.
- [15] F. Leach, M. Davy, M. Henry, M. Tombs, and F. Zhou, "A New Method for Measuring Fuel Flow in an Individual Injection in Real Time," in *SAE Technical Papers*, 2018, vol. 2018–April.
- [16] Henry, MP et al., "The Prism: Efficient Signal Processing for the Internet of Things," *IEEE Ind. Electron. Mag.*, vol. 11, no. 4, pp. 22–32, 2017.
- [17] Henry, MP. "The Prism: recursive FIR signal processing for instrumentation applications". *IEEE Transactions on Instrumentation and Measurement*, May 2019.
<http://dx.doi.org/10.1109/TIM.2019.2916943>
- [18] Henry, MP, Bushuev, O, Ibryaeva, O. "Prism Signal Processing for Sensor Condition Monitoring", 26th IEEE International Symposium on Industrial Electronics, Edinburgh, UK, 2017. DOI: 10.1109/ISIE.2017.8001451
- [19] Henry, MP, Sinitsin, V. "Prism Signal Processing for Machine Condition Monitoring I: Design and Simulation", 1st IEEE International Conference on Industrial Cyber-Physical Systems (ICPS-2018), May 2018.

- [20] Henry, MP, Sinitsin, V. "Prism Signal Processing for Machine Condition Monitoring II: Experimental Data and Fault Detection", 1st IEEE International Conference on Industrial Cyber-Physical Systems (ICPS-2018), May 2018.
- [21] M. P. Henry, "Ultra narrowband filtering with Prism signal processing: design and simulation," IEEE IECON 2018, vol. 1, no. October, pp. 2748–2753, 2018.
- [22] J. Owen, "384 TMAC / s FIR filtering on an Artix-7 FPGA using Prism signal processing," IECON 2018 - 44th Annu. Conf. IEEE Ind. Electron. Soc., vol. 1, pp. 2659–2664, 2018.
- [23] Clark C, Cheesewright R, Wang S. "Prediction of the Dynamic Performance of Fast Response Coriolis Meter Systems". IEEE Trans Instrum Meas. 2008;57(1):95-99.
- [24] Leach F, Davy M, Henry M, et al. "Fast NGC: A New On-Line Technique for Fuel Flow Measurement". SAE Technical Paper 2019-01-0062, 2019. doi:10.4271/2019-01-0062.
- [25] Li, M, Henry, M, "Complex signal processing for Coriolis mass flow metering in two-phase flow", Flow Measurement and Instrumentation, 64(2018), 104-115.
- [26] R. Smith, D. R. Sparks, D. Riley and N. Najafi, "A MEMS-Based Coriolis Mass Flow Sensor for Industrial Applications," in IEEE Transactions on Industrial Electronics, vol. 56, no. 4, pp. 1066-1071, April 2009.
- [27] Lötters, J.; Lammerink, T.; Groenesteijn, J.; Haneveld, J.; Wiegerink, R. "Integrated Thermal and Microcoriolis Flow Sensing System with a Dynamic Flow Range of More Than Five Decades". Micromachines 2012, 3(1), 194-203; <https://doi.org/10.3390/mi3010194>.

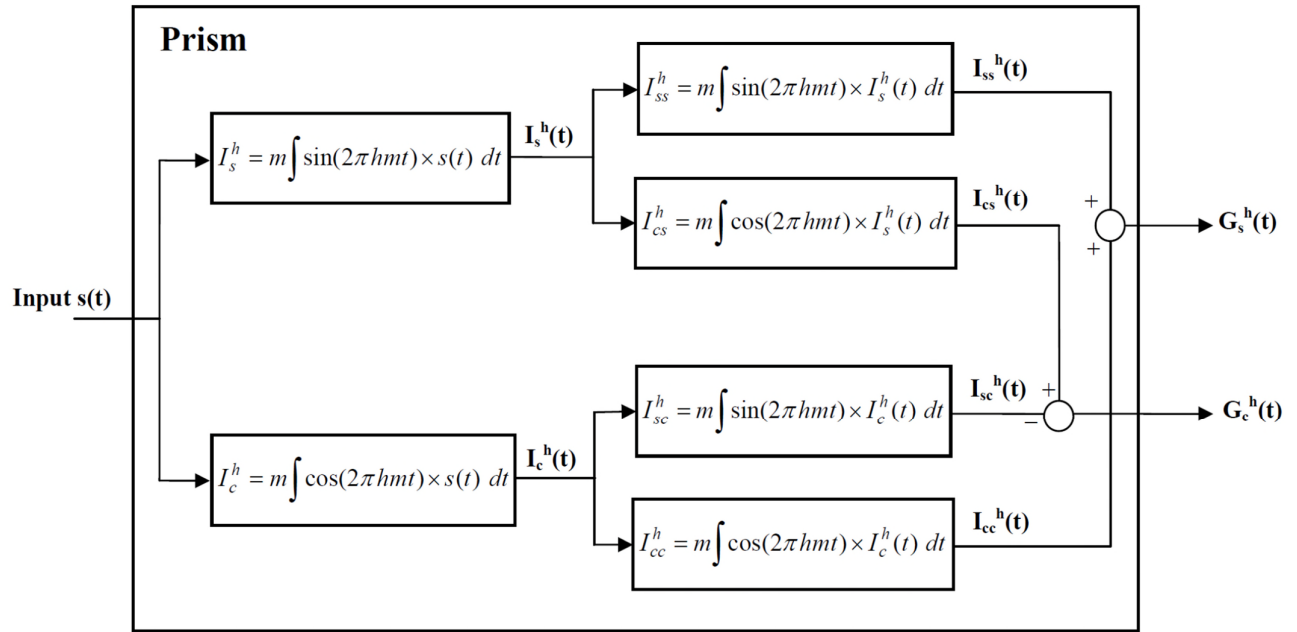


Fig. 1. Prism signal processing block with time series input $s(t)$ and time series outputs $G_s^h(t)$ and $G_c^h(t)$.

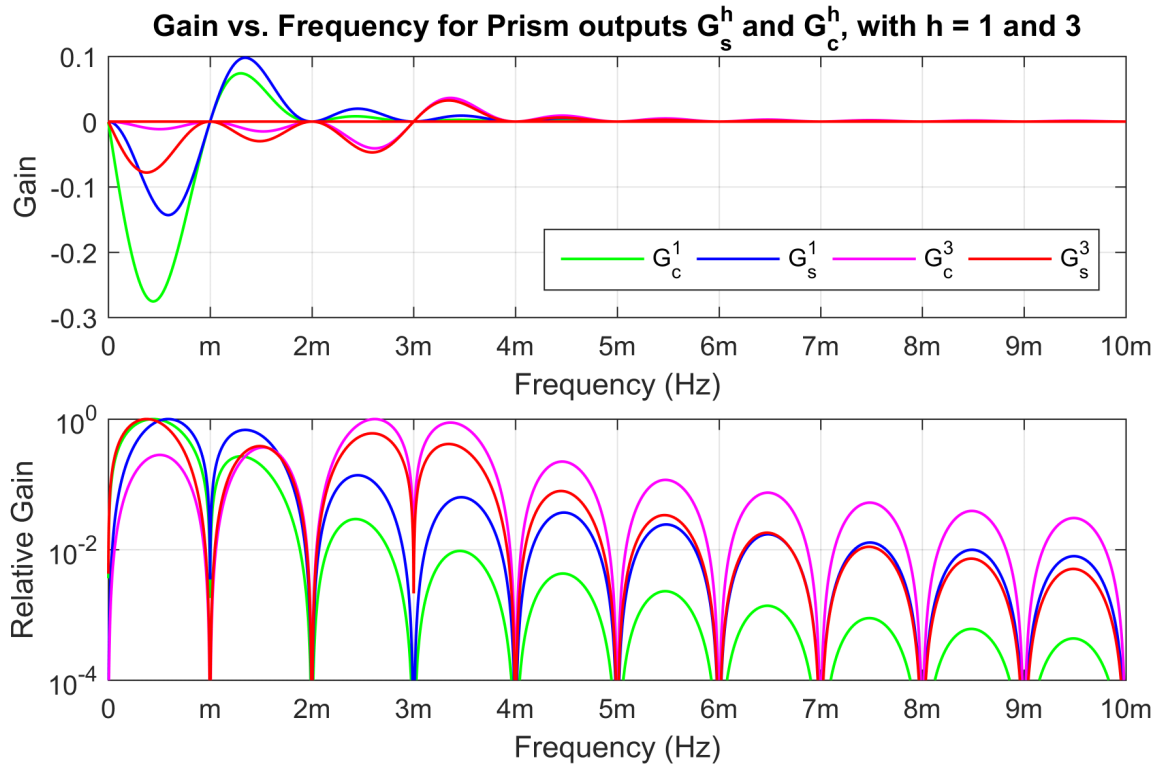


Fig. 2. Gains of Prism outputs. The relative gain is scaled against the peak (absolute) value for each function.

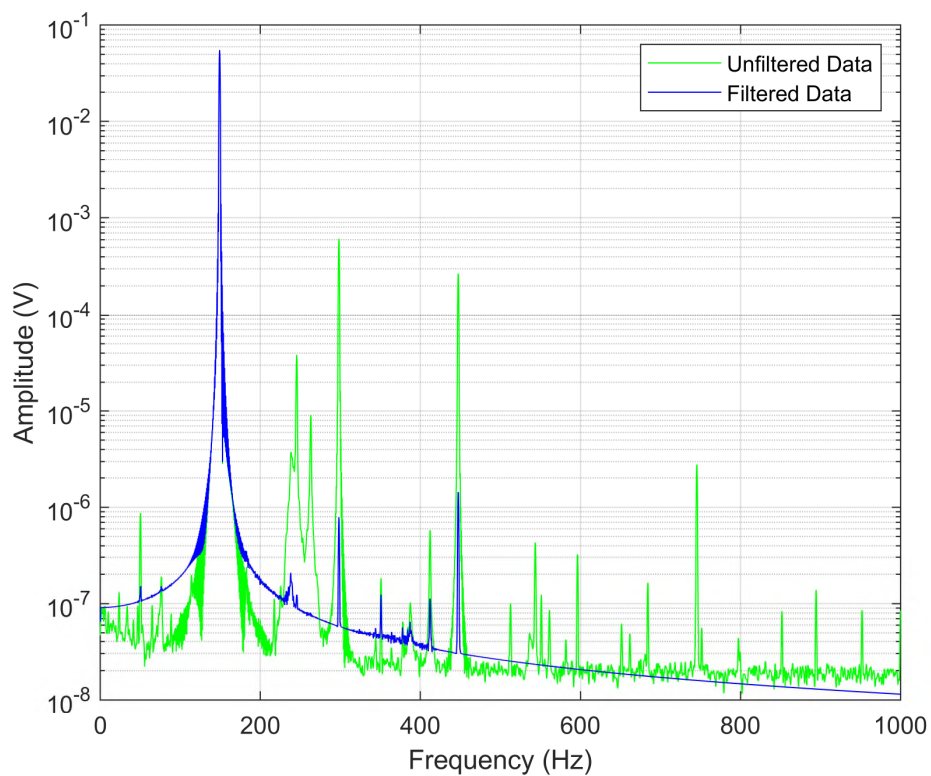


Fig. 3. Unfiltered and filtered Coriolis meter sensor spectrum at zero flow for high pressure flow tube.

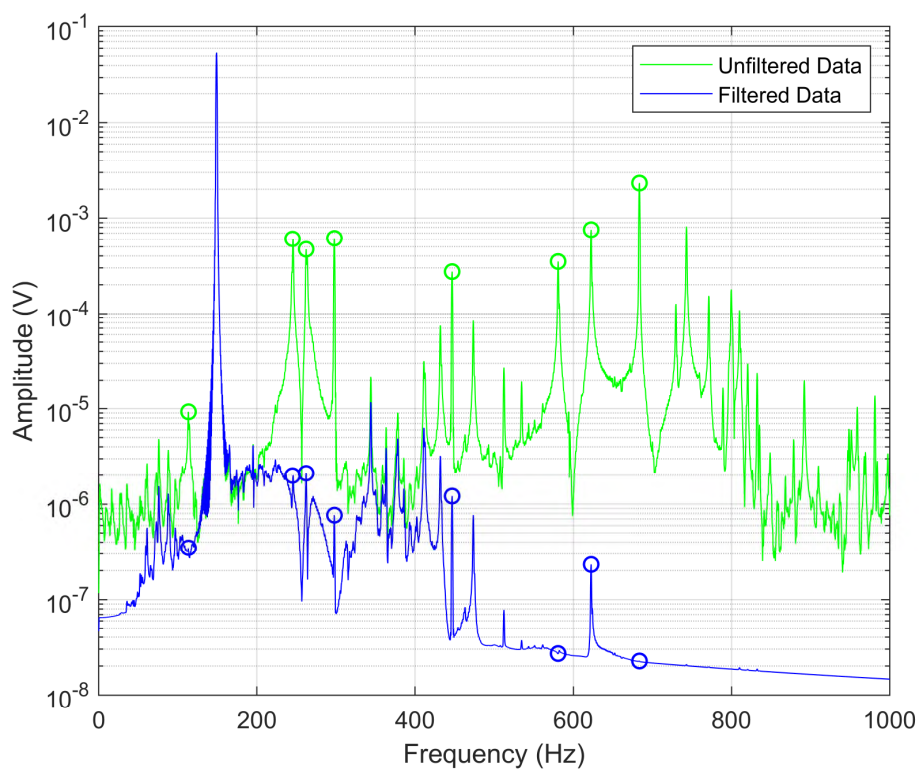


Fig. 4. Unfiltered and filtered Coriolis meter sensor spectrum during fuel injection pulse stream. Marked peaks are notch filter targets.

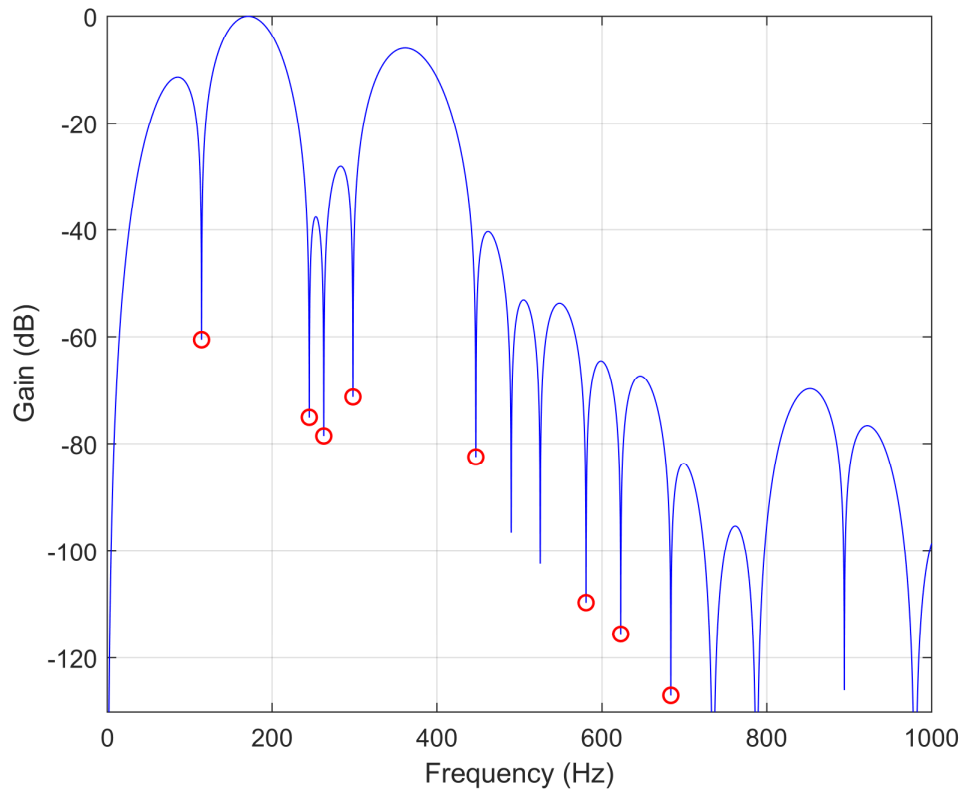


Fig. 5. Notch filter design for gasoline fuel injection experiments. Marked frequencies are notch targets.

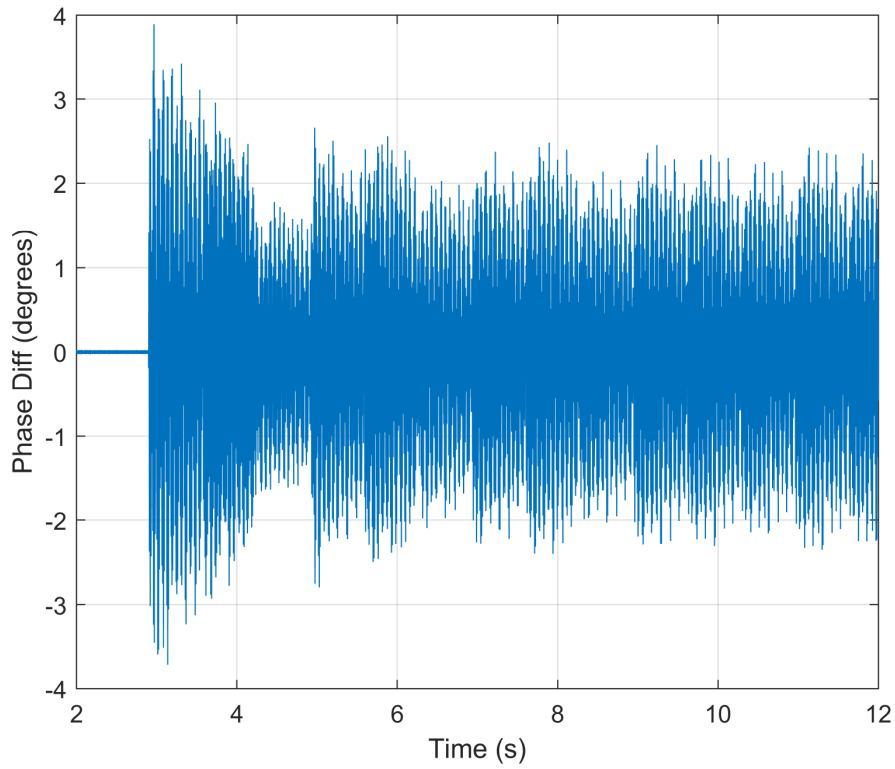


Fig. 6. Calculated phase difference based on the unfiltered data of Fig. 4.

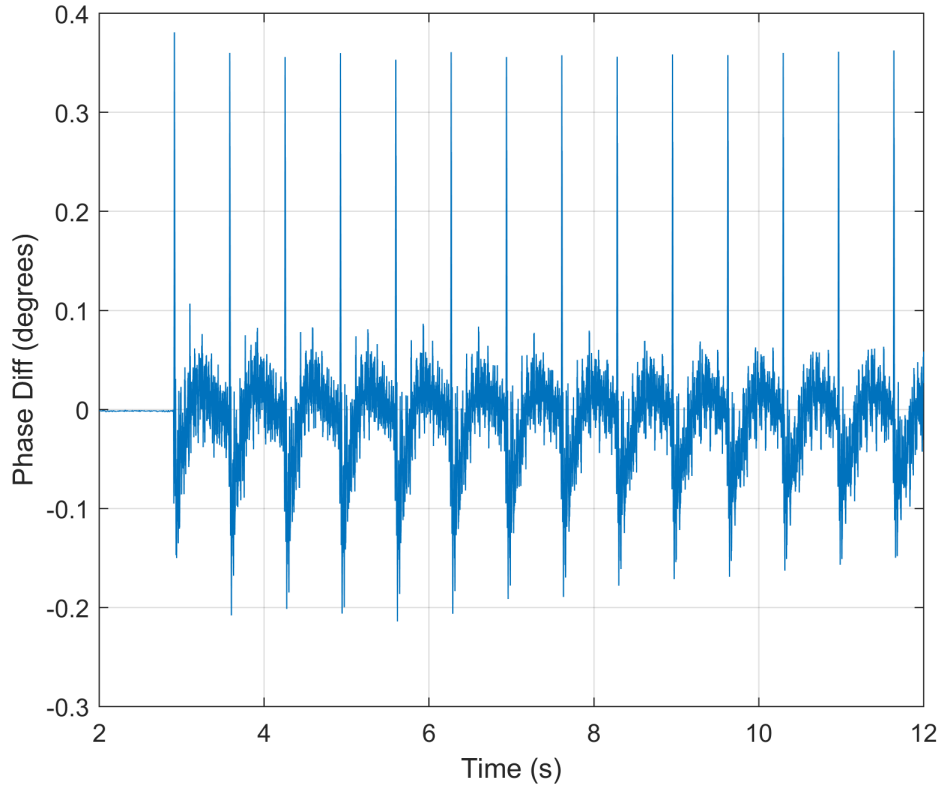


Fig. 7. Calculated phase difference based on the filtered data of Fig. 4.

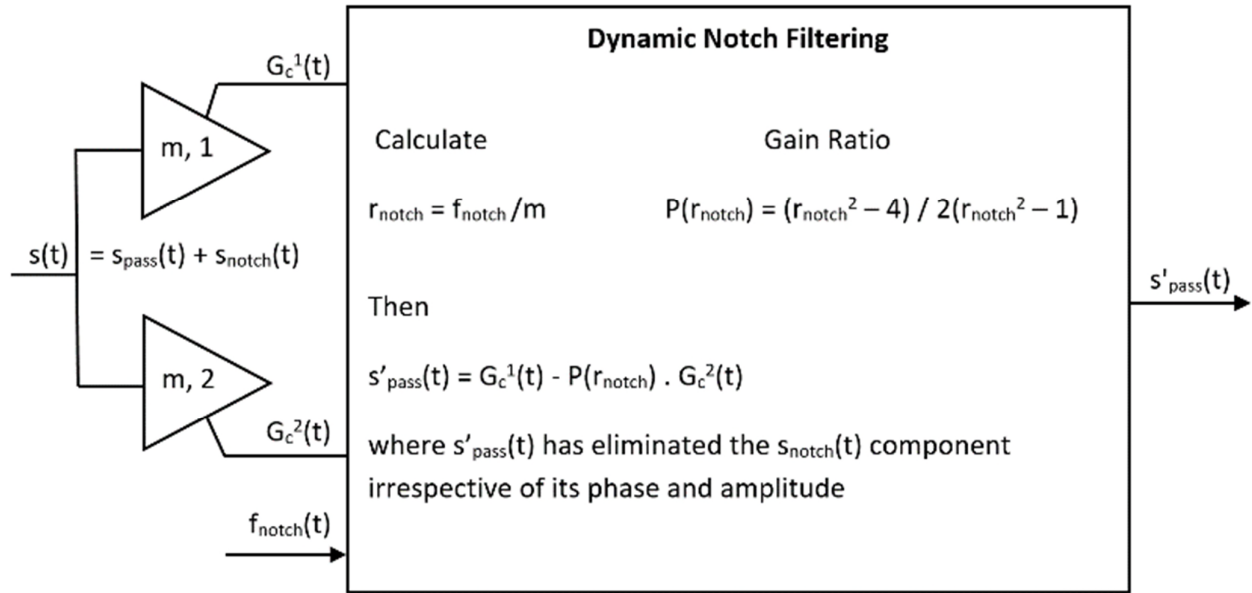


Fig. 8. Dynamic Notch Filtering (adapted from [21]).

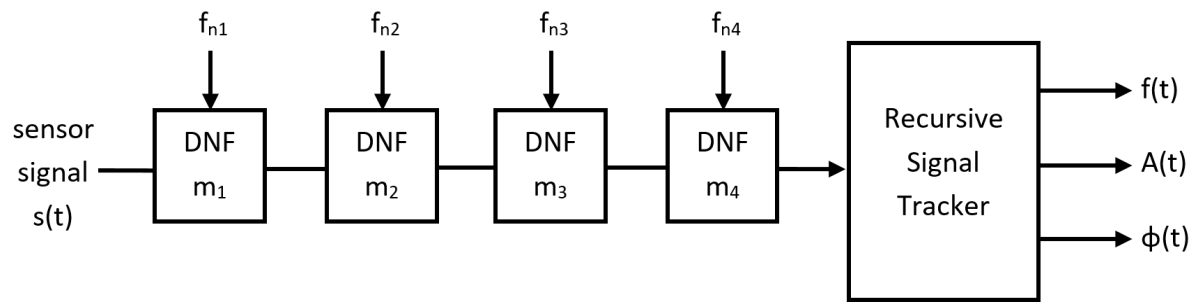


Fig. 9. Fuel injection Coriolis filtering and tracking scheme with four DNF stages

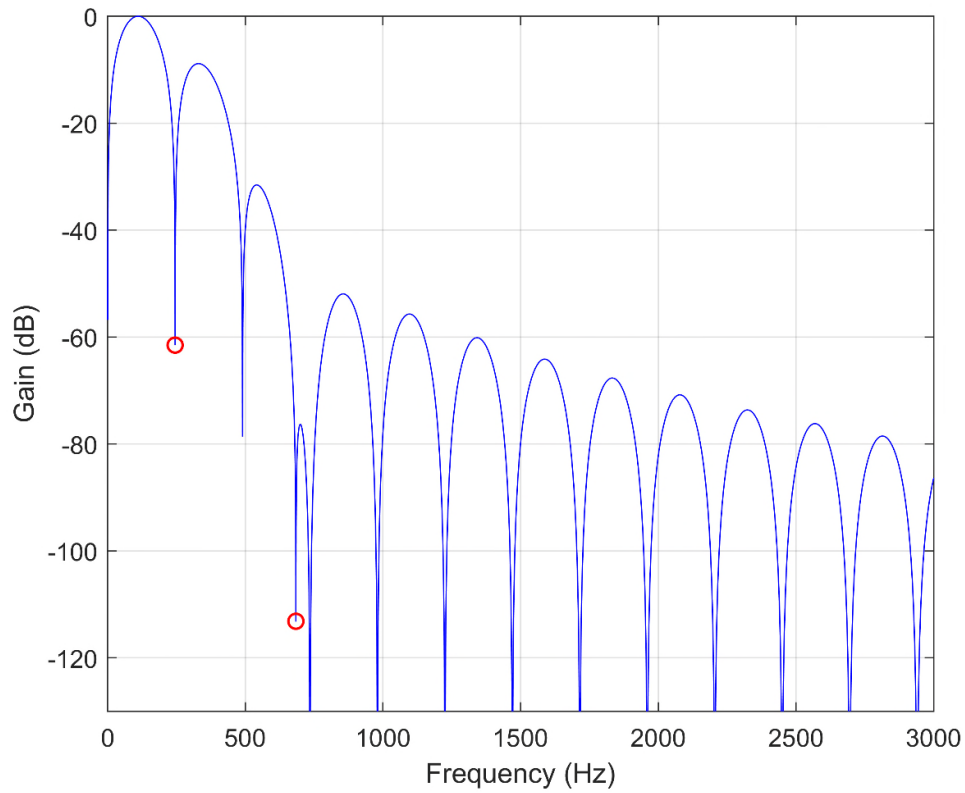


Fig. 10. Frequency response of first DNF stage. Marked frequencies are 245.0 Hz and 683.7 Hz

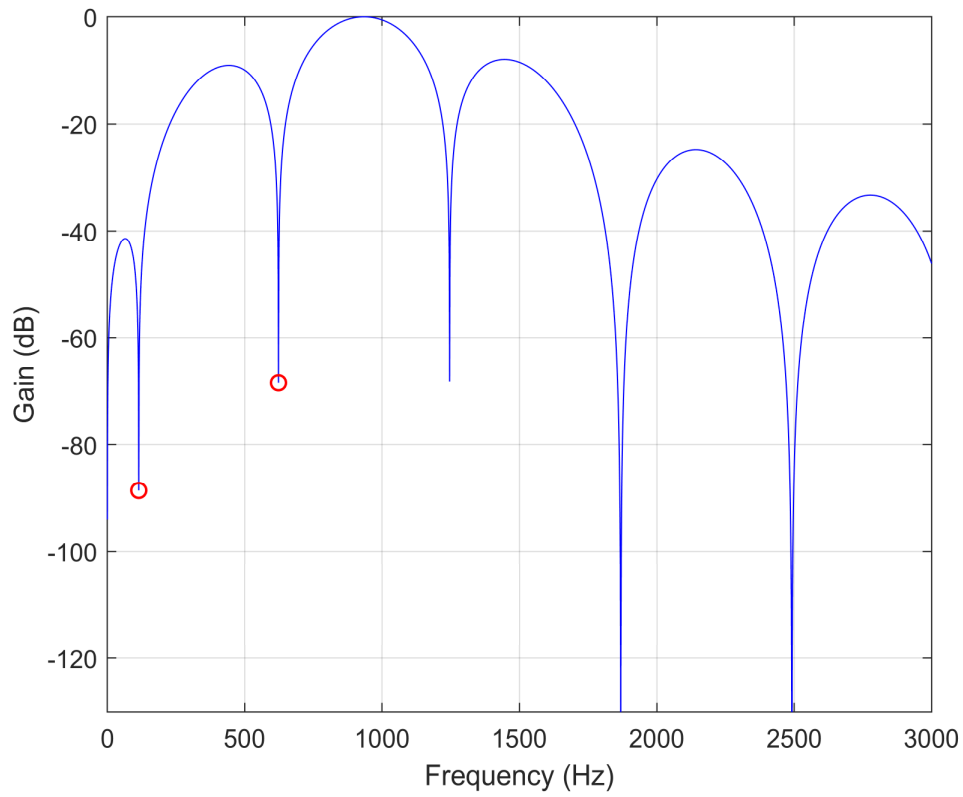


Fig. 11. Frequency response of fourth DNF stage. Marked frequencies are 114.3 Hz and 622.9 Hz

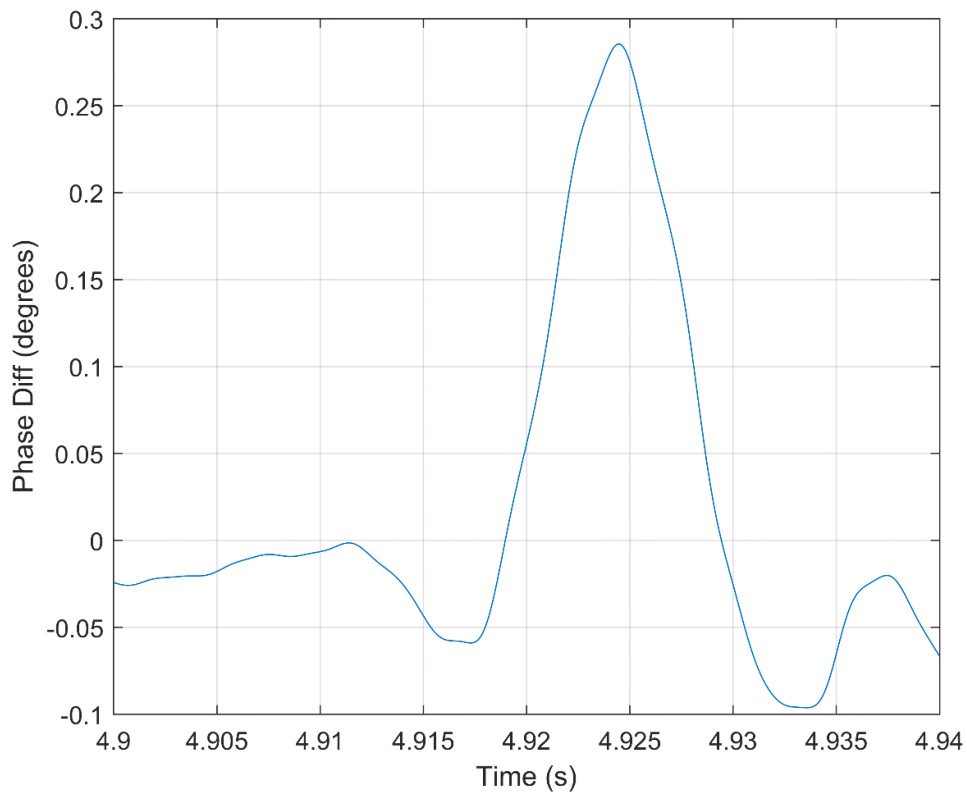


Fig. 12. Detail of phase difference measurement over an individual fuel pulse (from Fig. 7)

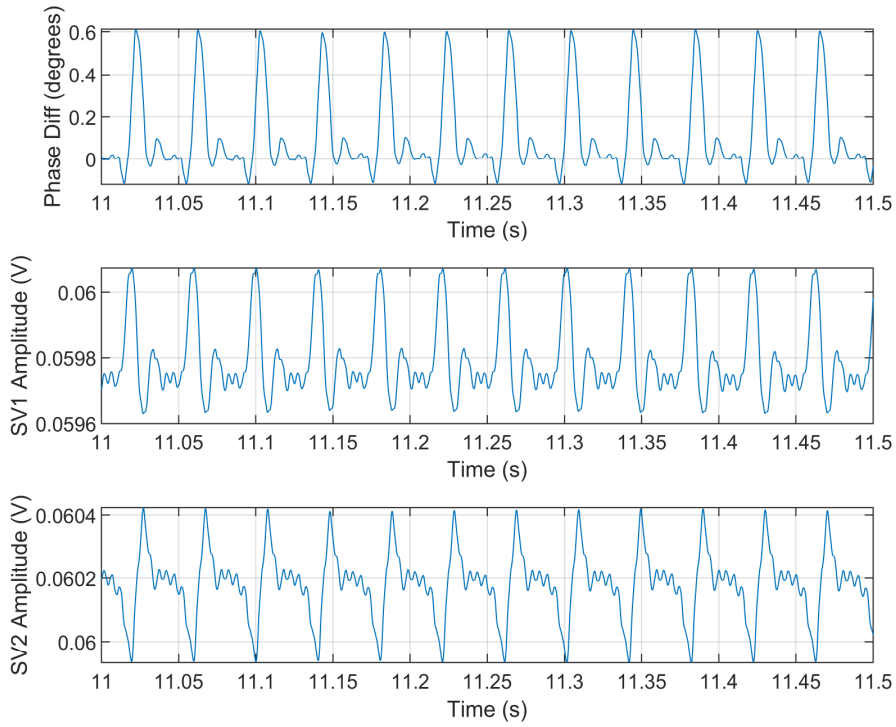


Fig. 13. Phase difference and sensor amplitude with pulse interval of 40.3 ms: data set 1

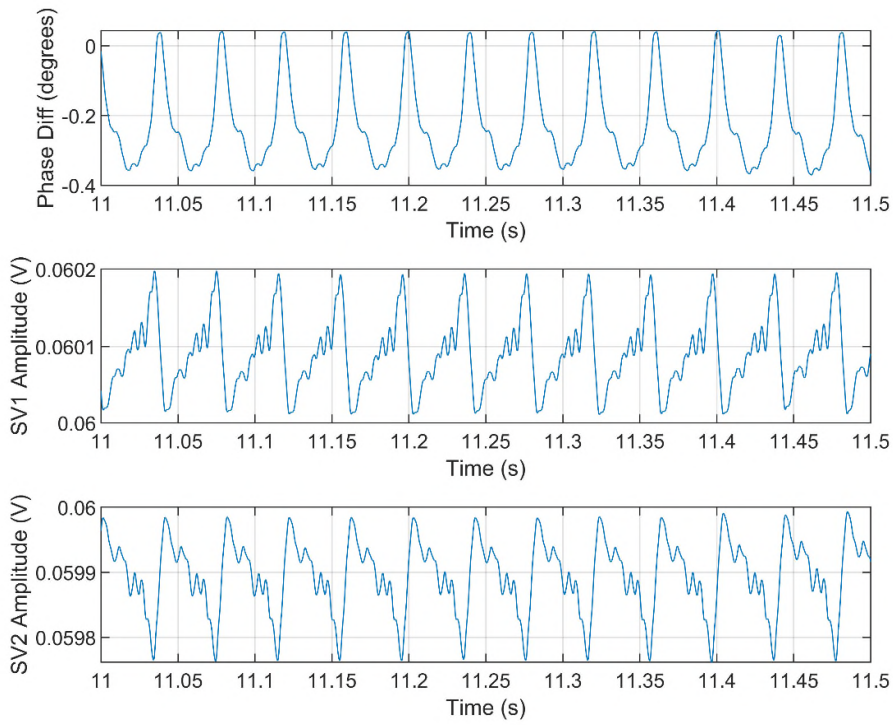


Fig. 14. Phase difference and sensor amplitude with pulse interval of 40.3 ms: data set 2

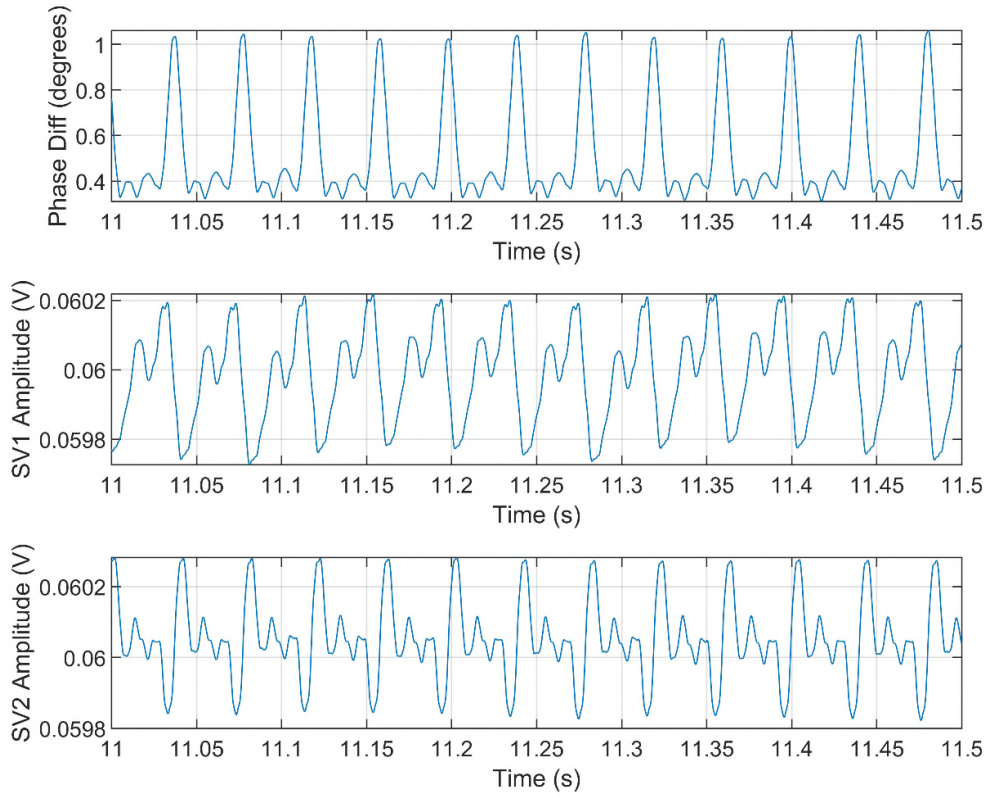


Fig. 15. Phase difference and sensor amplitude with pulse interval of 40.3 ms: data set 3

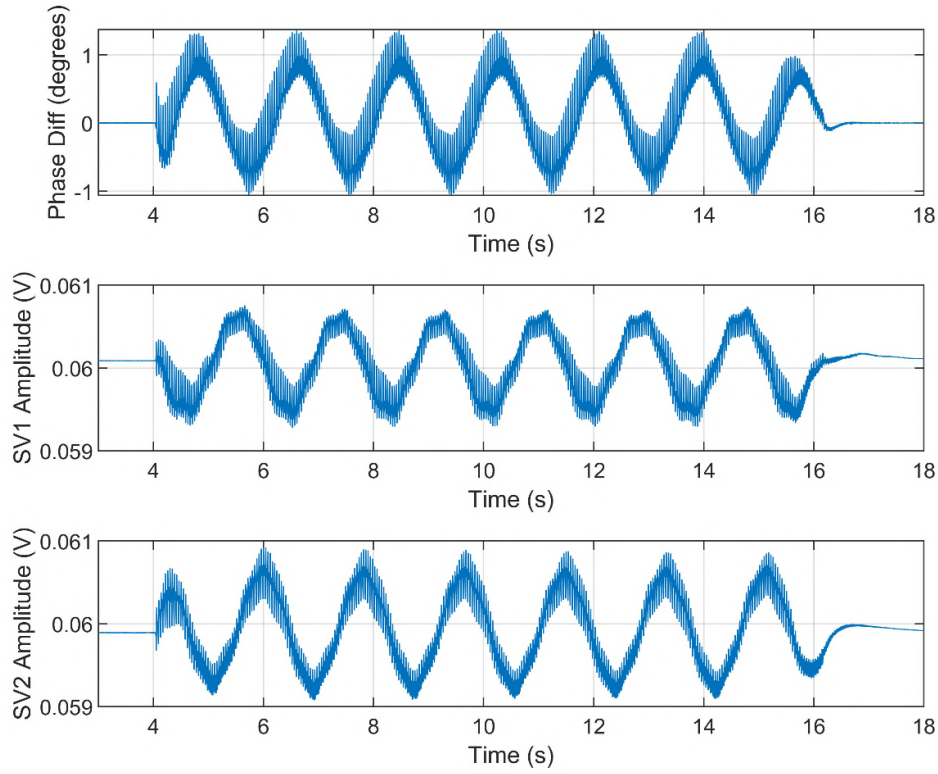


Fig. 16. Phase difference and sensor amplitude from 300 fuel pulses with pulse interval of 40.6 ms

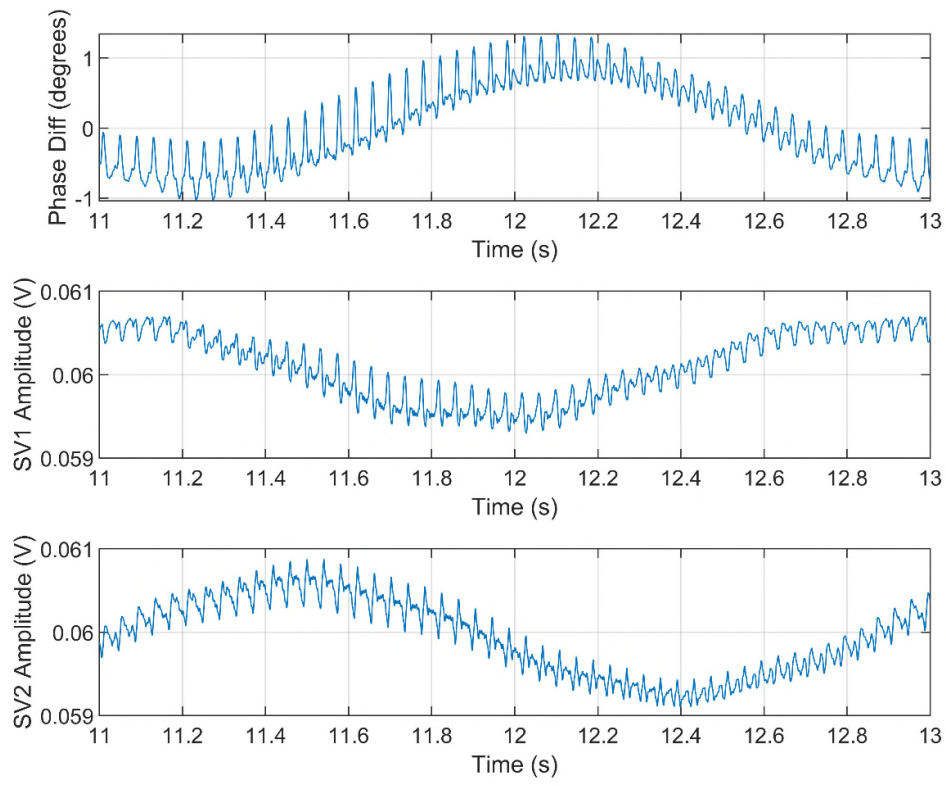


Fig. 17. Phase difference and sensor amplitude from 300 fuel pulses with pulse interval of 40.6 ms (detail)